Lateral MoS_2 p–n Junction Formed by Chemical Doping for Use in High-Performance Optoelectronics

Min Sup Choi,[†,‡] Deshun Qu,[†,‡,§] Daeyeong Lee,[†,‡,§] Xiaochi Liu,[†,‡,§] Kenji Watanabe,[∥] Takashi Taniguchi,[∥] and Won Jong Yoo[†,‡,§,*]

[†]SKKU Advanced Institute of Nano-Technology (SAINT), [‡]Center for Human Interface Nano Technology (HINT), and [§]Samsung-SKKU Graphene Center (SSGC), Sungkyunkwan University, 2066, Seobu-ro, Jangan-gu, Suwon, Gyeonggi-do 440-746, Korea, and [∥]National Institute for Materials Science, 1-1 Namiki, Tsukuba, Ibaraki 305-0044, Japan

ABSTRACT This paper demonstrates a technique to form a lateral homogeneous 2D MoS_2 p–n junction by partially stacking 2D h-BN as a mask to p-dope MoS_2. The fabricated lateral MoS_2 p–n junction with asymmetric electrodes of Pd and Cr/Au displayed a highly efficient photoresponse (maximum external quantum efficiency of ~7000%, specific detectivity of ~5×10^{10} Jones, and light switching ratio of ~10^3) and ideal rectifying behavior. The enhanced photoresponse and generation of open-circuit voltage (V_{OC}) and short-circuit current (I_{SC}) were understood to originate from the formation of a p–n junction after chemical doping. Due to the high photoresponse at low V_D and V_G attributed to its built-in potential, our MoS_2 p–n diode made progress toward the realization of low-power operating photodevices. Thus, this study suggests an effective way to form a lateral p–n junction by the h-BN hard masking technique and to improve the photoresponse of MoS_2 by the chemical doping process.

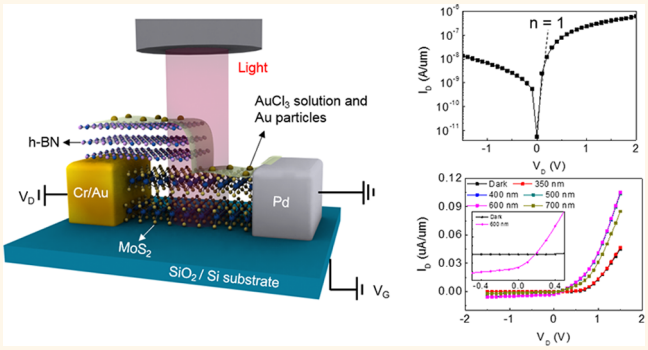

KEYWORDS: molybdenum disulfide · two-dimensional materials · chemical doping · lateral junction · homogeneous p–n junction · optoelectronics

The preparation of ultrathin graphene layers through mechanical exfoliation techniques has inspired extensive studies of other two-dimensional (2D) materials with a variety of electrical properties, including semiconducting molybdenum disulfide (MoS_2) and insulating hexagonal boron nitride (h-BN).[1−3] In particular, the semiconducting 2D material MoS_2 is potentially useful in post-silicon digital electronics due to its extreme thinness and also in highly efficient optoelectronics due to its tunable band gap and photocurrent. These 2D materials may be used to form the vertical heterostructures that are useful in a diverse range of functional devices, such as tunneling field effect transistors (FETs),[4,5] optoelectronics,[6,7] complementary inverters,[8] and memory devices.[9,10] These 2D materials could potentially replace Si-based devices and facilitate the development of next-generation flexible transparent electronics.[5,7,11] This potential may be realized through the development of appropriate doping processes because most useful devices include a variety of junctions (*e.g.*, p–n for diodes, p–n–p for MOSFETs, and p–i–n for tunnel transistors). The p–n diodes are particularly useful for optoelectronics because the built-in potential in the depletion region readily separates and drives the photogenerated e–h pairs that migrate toward the cathode and anode contacts and eventually generate a high photocurrent at a zero bias to enable efficient energy conversion. Therefore, high performances could be achieved in versatile Si-compatible electronics through the development of suitable doping methods for MoS_2. Several studies have examined surface charge transfer doping methods for MoS_2; however, it is unclear whether these methods can be applied toward the fabrication of practical junction devices because the electrical properties and contact resistance are only marginally modulated.[12−17]

* Address correspondence to yoowj@skku.edu.

Received for review June 17, 2014 and accepted August 17, 2014.

Published online August 18, 2014
10.1021/nn503284n

On the other hand, studies of the MoS_2 photoresponse have suggested new routes to the development of highly efficient optoelectronics. MoS_2 exhibits strong light absorption properties associated with Van Hove singularities in the density of state, and the visible range band gap can be as large as 1.9 eV for monolayer and 1.2 eV for multilayer MoS_2.[7,18] Phototransistors prepared using MoS_2 and heterostructured devices combined with graphene or carbon nanotubes have provided exceptionally high efficiencies and photoresponsivities.[6,7,19−24] By contrast, graphene phototransistors display a poor external quantum efficiency (EQE) of ∼1% and a photoresponsivity of ∼1 mA/W because the light absorption profile is weak and electron−hole recombination is rapid due to the zero band gap and fast carrier transfer.[25−28]

Here, we demonstrated the chemical preparation of p-type MoS_2 using a $AuCl_3$ solution and the use of this material in a lateral homogeneous p−n diode to yield a strong photoresponse. The fabricated p−n diode showed a high EQE, photoresponsivity, specific detectivity (D^*), and light switching ratio (I_{light}/I_{dark}) and an ideal rectifying behavior. Indeed, this p−n diode displayed unique properties, such as an open-circuit voltage (V_{OC}) and short-circuit current (I_{SC}) of typical of p−n diodes. These results suggest a new route to the application of MoS_2 toward numerous electronics using p−n junctions, such as rectifiers, Zener diodes, tunnel diodes, light-emitting diodes (LEDs), photodetectors, and solar cells.

RESULTS AND DISCUSSION

Formation of h-BN-Masked MoS_2 p−n Junction. The processes used to fabricate a representative MoS_2 p−n diode are described in Figure 1 (see the Experimental Methods for details). Mechanical exfoliation by adhesive tape produced multilayer MoS_2, which was then placed on a highly p-doped Si substrate covered by a thermally oxidized 280 nm SiO_2 layer. A portion of the MoS_2 surface area was p-doped by $AuCl_3$, and the remaining area was capped by h-BN using a transfer technique as reported previously.[3,29] The cross-sectional diagram and optical microscopy (OM) image of the MoS_2 p−n diode fabricated by spin-coating the $AuCl_3$ solution onto a partially stacked MoS_2/h-BN heterostructure are shown in Figure 1a and b. $AuCl_3$ can act as an effective electron acceptor due to its large positive reduction potential; thus, it is commonly used in studies of graphene doping.[30,31] It is known that the Au nanoaggregates formed through the reduction of $AuCl_4^-$ ions from solution. During this reaction, ions receive electrons from the MoS_2 layer, thereby leading to a significant p-doping of the MoS_2 through surface charge transfer. This formation of Au aggregates on the MoS_2 surface could be more clearly visualized using atomic force microscopy (AFM) (see the Supporting Information Figure S1).

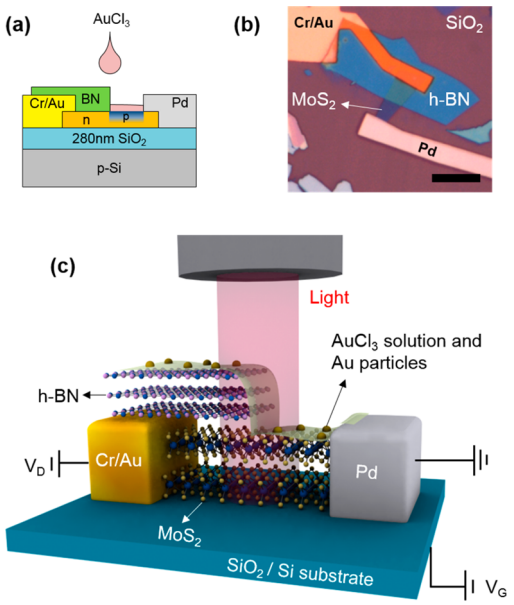

Figure 1. Fabrication of the MoS_2 p−n diode. (a) Cross-sectional diagram and (b) OM image of MoS_2 p−n diode with heteroelectrodes. The scale bar indicates 10 μm. (c) Three-dimensional schematic and circuit diagrams of the fabricated MoS_2 p−n diodes under light illumination.

Graphene is strongly impermeable, even with single atomic thickness, due to its dense honeycomb crystal lattice structure with very short C−C bond lengths.[32] As with the similar crystal structure of graphene, a several 10 nm thick h-BN layer completely blocks the large gold chloride ions from permeating; thus, the only exposed MoS_2 region appears to be p-doped by $AuCl_3$ and the remainder maintains its intrinsic n-type properties. The presence of different doped regions of the MoS_2 layer formed a lateral homogeneous p−n junction diode. By comparison with the conventional photoresist process, the use of h-BN as hard mask gives rise to some benefits: (i) superior impermeability with nanoscale thickness; (ii) facility to form an abrupt junction due to its thinness; (iii) simplified experimental process and reliability due to an unnecessary mask removal. Although the only surface region of MoS_2 is doped by surface charge transfer, it is expected that the p−n junction characteristics might be observed because the main current should flow along the upper side of multilayer MoS_2.[33] Thus, we investigated the electrical and optical properties of various thickness MoS_2 p−n diodes to find the layer dependence of chemical doping and optimal thickness. Three-dimensional schematic and circuit diagrams of the fabricated MoS_2 p−n diode are presented in Figure 1c. The Fermi energy (E_F) of MoS_2 could be tuned by applying a global back-gate bias to the Si substrate.

Rectification by Using Asymmetric Electrodes. Prior to the fabrication of the lateral MoS_2 p−n diode, we investigated the electrical properties and chemical doping effects of MoS_2 transistors with the electrodes of Ti/Au,

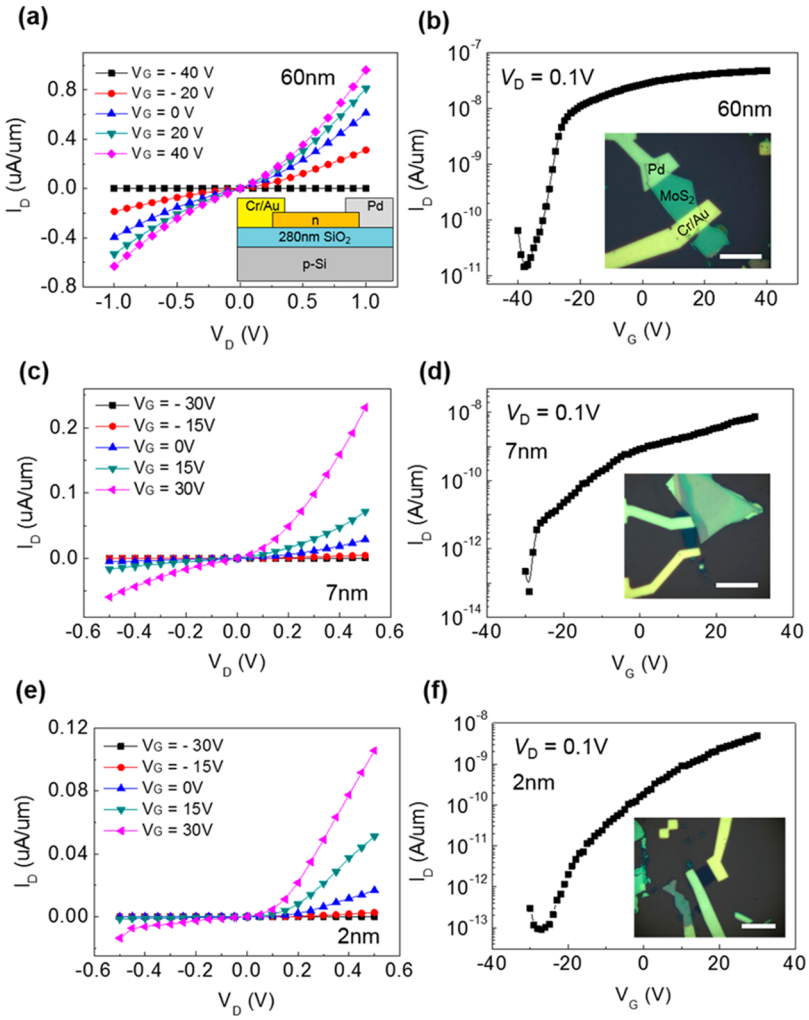

Figure 2. Electrical properties of MoS_2 transistors with a heteroelectrode. (a) I_D-V_D and (b) I_D-V_G curves of a 60 nm thick MoS_2 transistor. The inset in (a) shows a schematic diagram of the device. (c) I_D-V_D and (d) I_D-V_G curves of a 7 nm thick MoS_2 transistor. (e) I_D-V_D and (f) I_D-V_G curves of a 2 nm thick MoS_2 transistor. The insets in (b), (d), and (f) are OM images of each device, and the scale bars indicate 20 μm.

Cr/Au, and Pd as shown in Supporting Information Figures S2 and S3. The benzyl viologen (BV) and $AuCl_3$ showed effective n- and p-doping effects resulting in a degenerate n-type property and a p-type semiconducting property, respectively. In particular, with the large work-function Pd electrode, a MoS_2 transistor showed the obvious p-type semiconducting property after $AuCl_3$ doping. The on/off ratio and field effect mobility were comparable to those obtained prior to doping, and the V_T shift toward a negative gate bias was large (see Table S1). The low I_D and electron concentration at zero V_G provide clear evidence for the strong p-doping of $AuCl_3$.

With this experimental observation, we fabricated the various thickness MoS_2 transistors with a heteroelectrode (Pd−Cr/Au) to facilitate the flow of hole carriers from the p-doped region as described in the inset of Figure 2a. As shown in Figure 2, the electrical properties were changed depending on the thickness of MoS_2. For the thicker MoS_2 (30 and 60 nm), I_D-V_D showed a symmetric behavior even though different electrodes were contacted (Figure 2a and Supporting Information Figure S5a). This observation is quite different from Fontana *et al.*'s previous report.[23] They demonstrated the asymmetric I_D-V_D by just contacting different metals (Au−Pd) for S/D electrodes of 50 nm thick MoS_2. The different observations probably arose from the different fabrication processes, *e.g.*, different deposition methods. By contrast with thicker MoS_2, the thinner (2 and 7 nm) MoS_2 showed asymmetric I_D-V_D behaviors and lower current due to the induced Schottky barrier between the MoS_2 and Pd contact, as shown in Figure 2c and e. As reported in ref 23, in our case, the only thin MoS_2 below 7 nm showed asymmetric I_D-V_D by just contacting different metals. It seems that this effect became more significant as the thickness decreases. The I_D-V_G curves in Figure 2b, d, and f showed a significant threshold voltage (V_T) shift toward positive V_G direction from −30 to +10 V as the thickness decreases. The shift is attributed to the

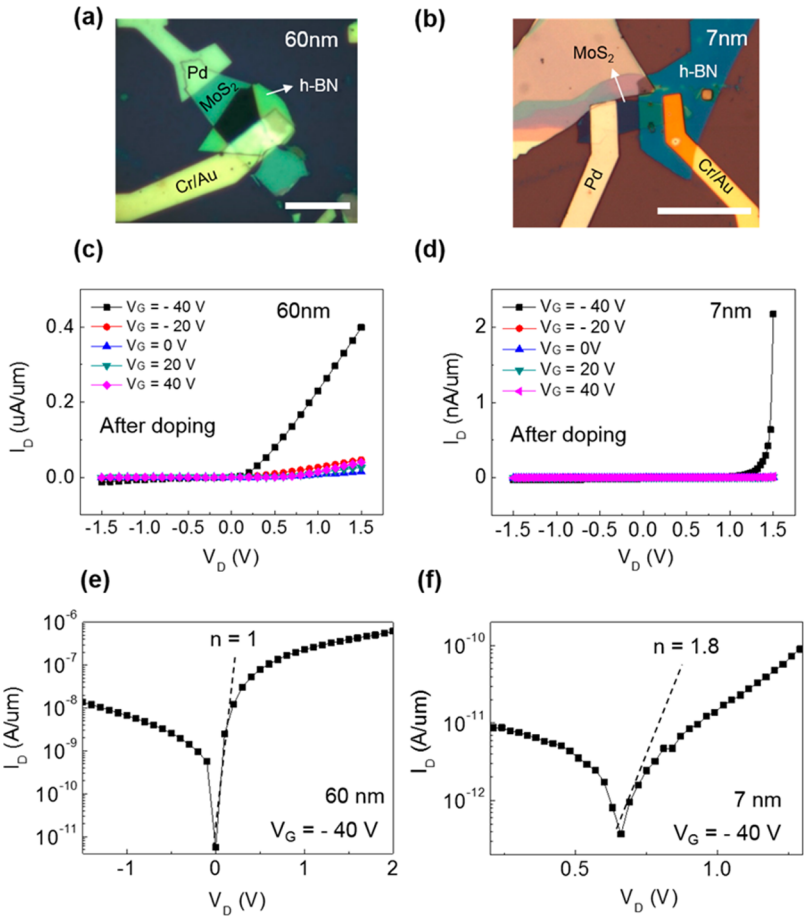

Figure 3. Electrical and diode performances of lateral MoS_2 p−n diodes. OM images for (a) 60 nm (PN-M60) and (b) 7 nm (PN-M07) thick MoS_2 p−n diodes. The scale bars indicate 20 μm. I_D−V_D curves of (c) PN-M60 and (d) PN-M07 after $AuCl_3$ doping. (e) Log-scale I_D−V_D curves of (e) PN-M60 and (f) PN-M07 at V_G = −40 V to calculate the ideality factors.

p-doping of MoS_2 with a Pd contact, and this effect also became more sensitive with thinner MoS_2 because the only contacted surface area with Pd probably is p-doped. However, all the transistors showed similar n-type semiconducting properties and a weak rectifying behavior such as low $I_{forward}/I_{reverse}$ ratio (∼10) even for 2 nm thick MoS_2. Thus, it is required to develop a new method to fabricate an ideal and high-performance p−n diode.

Electrical Properties of MoS_2 p−n Diodes. Here, we devised a lateral and homogeneous MoS_2 p−n diode as described in Figure 3a and b by stacking h-BN on a part of MoS_2 and depositing $AuCl_3$. When the electrical properties of MoS_2 p−n diodes were investigated with different doping concentrations (3, 20, and 30 mM), it was observed that the higher concentration of $AuCl_3$ can induce higher rectification (see Supporting Information Figure S7). Thus, it appears to be possible to optimize the diode performances by controlling doping concentration and generate tunneling current, which can be induced by a significant band-bending, by depositing a very high doping concentration of $AuCl_3$. For this experiment, we used 20 mM $AuCl_3$ dopant to form the p−n junction because this showed good rectifying and photonic behaviors.

Figure 3c and d show the I_D−V_D for the fabricated 60 and 7 nm thick MoS_2 p−n diodes (denoted as PN-M60 and PN-M07, in which the numbers indicate the thicknesses of MoS_2), respectively. By comparing with I_D−V_D before doping (Figure 2a and c), the rectifying behavior became more obvious after doping. The obtained $I_{forward}/I_{reverse}$ ratio is enhanced from 1.5 to 30 for 60 nm and from 4.2 to 67 for 7 nm thick MoS_2. From the log-plotted I_D−V_D, the doping effect for a rectification can be clearly seen, as shown in Supporting Information Figures S4a and S5a. Despite the enhanced rectification, the reason for a high reverse current of thicker MoS_2 at high $-V_G$ can be explained by the large drift current with applying high $-V_G$, which moves the E_F toward valence band and facilitates the hole carrier transport. Thus, the reverse current can be decreased with increasing V_G, as shown in Supporting Information Figure S4b. Despite this high reverse current, we could obtain an ideal diode characteristic. The I_D−V_D curves at V_G = −40 V for PN-M60 and PN-M30 exhibit an ideality factor of ∼1, which indicates an ideal diode from the following Shockley

diode equation:

$$I = I_S(e^{V_D/nV_T} - 1)$$

where I is the diode current, I_S is the reverse bias saturation current, V_D is the voltage across the diode, n is the ideality factor, and V_T is the thermal voltage (see Figure 3e and Supporting Information Figure S5b). This ideal diode characteristic probably is attributed to the homogeneous diode structure using the same material excluding the interface traps or unintended interface resistance, which can result in significant degradation of diode performances.

Furthermore, we analyzed the PN-M07 to obtain an ideality factor, as shown in Figure 3f. Despite its high $I_{forward}/I_{reverse}$ ratio, the ideality factor is higher than those of PN-M60 and PN-M30. It is known that the defects or interface traps that drive the recombination process would cause the ideality factor to be around 2. Thus, it seems that the thinner MoS_2 is strongly affected by the chemical solution or damaged during surface chemical reaction. The formation of Au aggregates also can prevent carrier transport, and this influence should be more dominant for the thinner MoS_2. In the case of PN-M02, I_D was significantly suppressed after $AuCl_3$ doping, and we observed that it could be recovered after rinsing in acetone for 1 day to remove the chemical solution (Supporting Information Figure S6). However, the recovered I_D was little lower than that of the pristine state. This observation demonstrates that the chemical solution or Au aggregates can significantly suppress the electrical conduction of thin MoS_2 below 7 nm and the defects can be generated during the chemical doping process. In a previous report, similar thinning-induced suppression of electrical conduction against the environmental condition was demonstrated.[34] In addition, the Schottky barrier formed at a thin MoS_2/Pd contact as mentioned in Figure 2 should induce the unintended contact resistance. Thus, the rectifying behavior should be attributed to both the p−n junction and Schottky barrier. We think that this contact resistance also can give rise to the higher ideality factor, compared with that of thick MoS_2. As a result, the influences of Au nanoaggregates, defects, and contact resistance at the Schottky barrier hamper the formation of an ideal p−n junction for the thin MoS_2. It is required to find the optimized thickness and proper chemical doping process for thin-layer MoS_2 in further studies. For detailed information and a summary of fabricated MoS_2 p−n diodes, see the Supporting Information Table S2.

Photoresponses of MoS_2 p−n Diodes. An important application of p−n diodes is the fabrication of photodevices. We measured the photocurrent at different V_G generated upon monochromatic light illumination (wavelength ranging from 300 to 700 nm) for a PN-M60, which showed an ideal diode characteristic, as shown in Figure 4. Before doping, I_D-V_D showed different on-and-off states as shown in Figure 4a and b, respectively. This indicates a typical n-type semiconducting property. At on-state, it is very difficult to distinguish the dark current (I_{dark}) and light current (I_{light}) since a lot of accumulated carriers at high $+V_G$ considerably contribute to the total channel current. Thus, it is not suitable for use as a photodetector at this

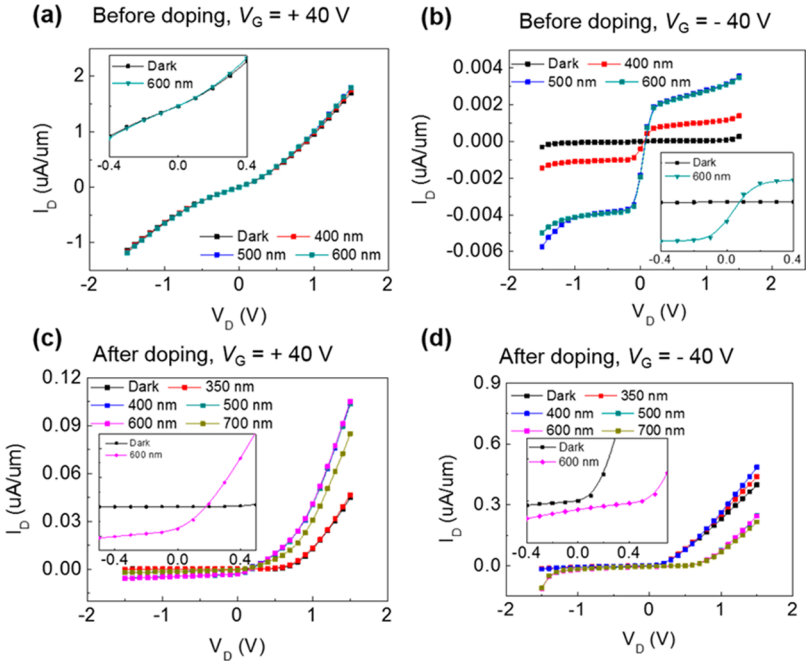

Figure 4. Photoresponse of PN-M60. (a, b) I_D-V_D before and (c, d) after $AuCl_3$ doping at different V_G. The insets show enlarged graphs to visualize the unique properties of the p−n diode such as open-circuit voltage and short-circuit current with exposure to 600 nm wavelength light.

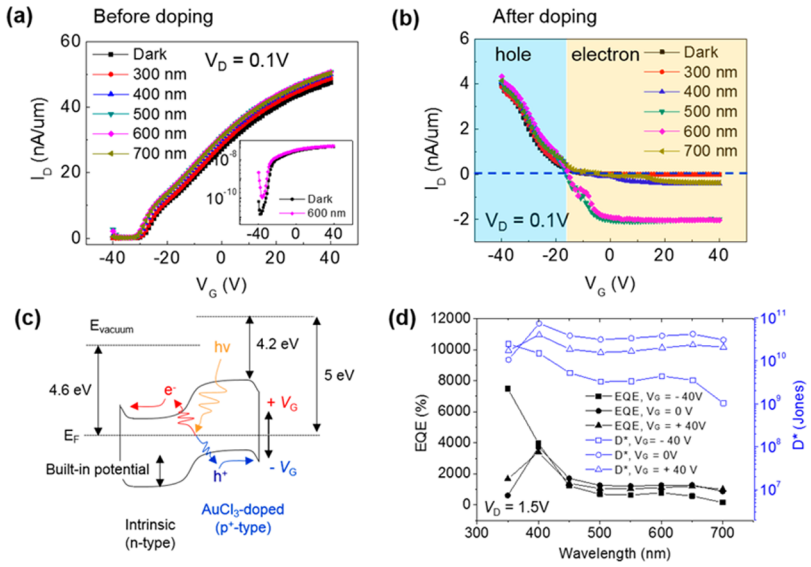

Figure 5. I_D-V_G of PN-M60 (a) before and (b) after $AuCl_3$ doping with light exposure. The wavelength of exposed light ranges from 300 to 700 nm. (c) Band diagram of a MoS_2 p−n diode with applying different V_G. (d) Calculated EQE and D^* with respect to the wavelength of light at $V_D = +1.5$ V and $V_G = 0, \pm 40$ V.

state. In contrast, at off-state we could clearly observe the I_{light} due to the very low I_{dark}. Interestingly, the unique properties of a p−n diode such as V_{OC} and I_{SC} were observed at this state, as shown in the inset of Figure 4b. We believe that the different electrodes (Pd and Cr/Au) for S/D contacts resulted in these properties. However, the V_{OC} and I_{SC} were just 0.08 V and 20.4 nA without the $AuCl_3$ doping process. Meanwhile, we also measured I_{light} after $AuCl_3$ doping, as shown in Figure 4c and d. By comparison with that before doping, I_{light} was more visible at both negative and positive V_G. The V_{OC} and I_{SC} were also enhanced to 0.2 V and 31.2 nA at $V_G = +40$ V and 0.5 V and 46.7 nA at $V_G = -40$ V after doping (see the insets). The same structured PN-M30 also showed similar electrical and photonic properties, as shown in Supporting Information Figure S5c. This manifests the clear advantage of a p−n junction photodevice over just an intrinsic photodevice as presented in many studies.[19−21] Furthermore, this possibly alludes to applicability for photovoltaic cells. Further experiments with an AM 1.5G solar measurement system will be studied.

Figure 5a and b indicate the I_D-V_G curves of PN-M60 before and after $AuCl_3$ doping, respectively. We applied low $V_D = 0.1$ V to investigate the V_G effect by excluding the huge drift or tunneling current induced by large V_D. Before doping, it showed a typical n-type semiconducting property and slight increase of current with light exposure. As described by the I_D-V_D in Figure 4, I_{light} is distinguishable at only negative V_G (see inset of Figure 5a), while it is difficult at positive V_G. Although it is distinguishable, the light switching ratio (I_{light}/I_{dark}) was just ~33 at $V_G = -40$ V. It is noted that the generated photocurrent is always positive at all tested V_G regions before doping. These behaviors are very similar to a previous study on a multilayer MoS_2 phototransitor.[21] In contrast, the MoS_2 p−n diode showed a quite different photoresponse after doping. First, we could divide the V_G regions in two: one is hole- ($+I_D$ at $-V_G$) and the other is electron-dominated ($-I_D$ at $+V_G$). It is known that V_G can be used to effectively control E_F in 2D materials. The applied positive V_G upshifts E_F in MoS_2, whereas a negative V_G downshifts E_F as shown in Figure 5c. The upshifted (downshifted) E_F at positive V_G (negative V_G) leads to additional electron (hole) accumulation and reduction of the barrier height between the conduction (valence) band edge of MoS_2 and the S/D contacts. As a result, the different applied V_G resulted in the different signs of I_{ph}. The reason for a shifted transition point ($-I_{light}$ to $+I_{light}$) at $V_G = -18$ V is probably dependent on the initial and $AuCl_3$-doped states of MoS_2. Second, we could obtain a very high light switching ratio compared to the intrinsic MoS_2. Especially, the $\sim 10^3$ light switching ratio (I_{dark} is 3×10^{-11} A and I_{light} at 500 nm is 2×10^{-8} A) can be observed even at zero V_G with small $V_D = 0.1$ V (intrinsic MoS_2 showed just a 1.15 light switching ratio at zero V_G and same V_D). It is understood that the high photoresponse at low voltage is attributed to the built-in potential, which readily separates and drives the photogenerated e−h pairs, induced by the formation of a p−n junction. Thus, our p−n diode is very useful for low-power operating photodetectors using a high switching ratio.

We evaluated the optical performances of PN-M60 by calculating the EQE and D^*, the following key parameters for photodevices:

$$\text{EQE}\,(\%) = \frac{hc}{e}\frac{I_{ph}}{P} \times 100$$

TABLE 1. Performance Comparison of Our MoS_2 p−n Diode with Intrinsic MoS_2 Phototransistors and Conventional ZnO/Si Photodiodes

device	measurement condition (wavelength, bias)	EQE (%)	photoresponsivity (A/W)	specific detectivity (Jones)	response time (ms)
our MoS_2 p−n diode	500 nm, $V_D = +1.5$ V, $V_G = 0$ V (forward)	1200	5.07	3×10^{10}	100−200
	$V_D = -1.5$ V, $V_G = 0$ V (reverse)	81	0.33	1.6×10^{10}	
intrinsic MoS_2 phototransistor[19,21]	530 nm, $V_D = +1$ V, $V_G = -3$ V	11.7	0.05	2×10^{10}	
	550 nm, $V_D = +1$ V		<0.01		50
conventional ZnO/Si photodiode[36−38]	530 nm, $V_D = -1$ V (reverse)	47.33	0.204		
	365 nm, $V_D = -2$ V (reverse)	25	0.075	6.44×10^{11}	
	670 nm, $V_D = +5$ V (reverse)	53	0.288		35×10^{-6}

$$R\,(A/W) = \frac{I_{ph}}{P}$$

and

$$D^*\,(\text{Jones}) = \frac{RA^{1/2}}{(2eI_{dark})^{1/2}}$$

where h is Planck's constant, c is the speed of light, I_{ph} is the photocurrent ($|I_{light} - I_{dark}|$) flowing through the effective device area, P is the power intensity per unit area, λ is the wavelength of the light, e is the unit charge, R is the photoresponsivity, and A is the area of the device.[21] The I_{ph} is extracted from the I_D-V_D curves in Figure 4. Our MoS_2 p−n diode yielded very high EQE values, as shown in Figure 5d. The calculated EQE value showed its maximum value, ~ 7000%, at V_D = 1.5 V, $V_G = -40$ V, and 350 nm. Although it tends to decrease with increasing wavelength, nearly 1000% is obtained under all tested V_G (notably even at zero V_G) and wavelengths. It should be noted that this high EQE at low V_D and zero V_G is remarkable. The D^* is a figure of merit for photodetectors, which indicates the measure of detector sensitivity. We could obtain a comparable D^*, ranging from 10^9 to 10^{11} Jones at all tested wavelengths and V_G, with a previous study on multilayer intrinsic MoS_2 phototransistors.[21] Thus, the sensitivity of our photodiode is independent of the $AuCl_3$ doping and stacking processes.

In order to achieve high EQE or photoresponsivity, the previous studies on MoS_2 phototransistors were investigated under very high V_G and V_D so as to induce the additional thermionic and tunneling charges and strongly drive photogenerated carriers.[19−21] However, our p−n diode offers exceptional benefits due to its innate built-in potential in a p−n junction, which help to separate and collect photocarriers at small V_D and zero V_G. On the other hand, it is known that the formation of Au nanoparticles also can enhance photoabsorption properties due to the plasmonic nanostructures.[7,35] We also tested the photonic effect of Au nanoaggregates formed after $AuCl_3$ doping; however, there is no significant enhancement of photoresponse in our experimental conditions (see the detailed experiment in Supporting Information Figure S8). This manifests that the enhanced photoresponse and low-power operation are attributed to the formation of a p−n junction.

To verify the benefits of a p−n junction, we evaluated the photonic parameters at low bias and reverse bias regimes. From the I_D-V_G curve (V_D = 0.1 V) in Figure 5b, the calculated EQE and light switching ratio are ~15% and ~10^3 at zero V_G, respectively. With applying a small V_D = 0.3 V and zero V_G, the extracted EQE and D^* reach ~100% and 5 × 10^{10} Jones at all tested wavelengths; thus this showed the possibility of low-power operating photodevices (see Supporting Information Figure S9a). In general, photodevices need to be operated at a reverse bias regime. At $V_D = -1.5$ V (reverse bias), the EQE and D^* showed ~80% and ~2 × 10^{10} Jones, as shown in Supporting Information Figure S9b. These values are relatively higher than those reported for 2D heterostructures[6,7,22,24] and conventional ZnO/Si photodiodes.[36−38] Note that the lateral homogeneous p−n diode has distinct advantages over the vertical heterostructures, which inevitably involve junction resistance between the two stacked materials. When the time-resolved photoresponse was measured, a reasonable response time (100−200 ms) could be observed both before and after $AuCl_3$ doping, as shown in Supporting Information Figure S10. These values are similar to the intrinsic MoS_2 (50 ms).[19] The lower response time than conventional ZnO/Si photodiodes (35 ns) is probably due to its lower carrier mobility (normally MoS_2 shows several 10 $cm^2/(V\ s)$). Thus, it is required to achieve high speed p−n diodes using high-mobility 2D materials, proper contacts, and high-k dielectrics in further studies. The summarized photonic parameters (EQE, R, D^*, and response time) and comparison with intrinsic MoS_2 phototransistors and conventional ZnO/Si photodiodes are shown in Table 1. Consequently, the superior efficiency of our MoS_2 p−n diode offers clear advantages with respect to the chemical doping method used to obtain high-performance MoS_2 optoelectronic devices.

CONCLUSION

The use of partially stacked h-BN on MoS_2 in combination with $AuCl_3$ doping successfully yielded lateral homogeneous MoS_2 p−n diodes. The fabricated devices showed an ideal rectifying behavior and a

strong photoresponse induced by the formation of a p−n junction. The obtained high EQE, *R*, *D**, and light switching ratio at zero V_G and low V_D demonstrated the possibility for use of low-power operating photodevices. In addition, the MoS_2 p−n junction displayed unique properties, such as open-circuit voltage and short-circuit current, suggesting that the diodes can provide applicability for photovoltaic cells. This study provides a promising approach to using chemically doped MoS_2 as a 2D material in post-silicon electronic and optoelectronic device applications.

EXPERIMENTAL METHODS

Synthesis of the Chemical Dopants of MoS_2. The BV dopant was prepared by dissolving 0.0164 g (20 mM) of 1,1′-dibenzyl-4,4′-bipyridinium dichloride (benzyl viologen, Sigma-Aldrich) powder in 5 mL of DI water. Then, 5 mL of toluene was added to create a biphasic phase. Sodium borohydride ($NaBH_4$, 200 mM) was also added as a reducing agent. The BV^{2+} ions were reduced and transferred from the water to the toluene phase. This toluene phase was extracted from the solution after 1 day. The synthesized BV dopant was spin-coated onto a MoS_2 layer at 2500 rpm for 1 min, followed by annealing at 100 °C for 10 min to obtain uniform coverage. The $AuCl_3$ dopant was prepared by dissolving 0.034 g (20 mM) of gold chloride ($AuCl_3$, Strem Chemicals) powder in 5 mL of nitromethane. For this dopant, the solution was sonicated and filtered to avoid the formation of unwanted large Au aggregates and to ensure dissolution. The post-annealing used for the BV dopant was also applied after $AuCl_3$ doping. The synthetic procedures have been described previously.[30]

Device Fabrication and Measurements. The MoS_2 flakes were prepared using the mechanical exfoliation method. The doped Si substrate beneath the 280 nm SiO_2 layer was used as a global back-gate. The p−n diode was fabricated by partially transferring h-BN onto the MoS_2 layer using a polydimethylsiloxane stamp. The metal electrodes (5/50 nm Ti/Au and Cr/Au, and 50 nm Pd) were formed using electron beam lithography and evaporation. The $AuCl_3$ chemical dopant was spin-coated onto the partially stacked h-BN/MoS_2 heterostructure, and post-treatments were applied to ensure uniform doping. The thicknesses and surface states of the MoS_2 and h-BN layers were verified by AFM. All electrical measurements were conducted using a semiconductor parameter analyzer (Agilent, 4155C) under ambient conditions except the low-temperature measurement for extraction of barrier height. The photocurrent was measured using a monochromatic light with various wavelengths ranging from 300 to 700 nm and an illumination diameter of 60 μm. The power of light was measured by an optical power meter. The details of the photoresponse measurement system are described in ref 39.

Conflict of Interest: The authors declare no competing financial interest.

Supporting Information Available: AFM images of MoS_2 before and after $AuCl_3$ doping (Figure S1); electrodes and chemical doping effects for the MoS_2 transistor (Figures S2, S3 and Table S1); electrical properties of various thickness MoS_2 p−n diodes (Figures S4−S6); doping concentration dependent rectification of MoS_2 p−n diodes (Figure S7); investigation on plasmonic effect of Au nanoaggregates (Figure S8); photonic properties of PN-M60 at low and reverse bias regimes (Figure S9); response time of the MoS_2 p−n diode before and after doping (Figure S10); information of MoS_2 p−n diodes (Table S2). This material is available free of charge *via* the Internet at http://pubs.acs.org.

Acknowledgment. This work is supported by the Basic Science Research Program and Global Ph.D. Fellowship Program through the National Research Foundation of Korea (NRF) (2009-0083540, 2012H1A2A1004044, and 2013-015516) and by the Global Frontier Program through the Global Frontier Hybrid Interface Materials (GFHIM) of NRF funded by the Ministry of Science, ICT & Future Planning (2013M3A6B1078873).

REFERENCES AND NOTES

1. Novoselov, K. S.; Geim, A. K.; Morozov, S. V.; Jiang, D.; Zhang, Y.; Dubonos, S. V.; Grigorieva, I. V.; Firsov, A. A. Electric Field Effect in Atomically Thin Carbon Films. *Science* **2004**, *306*, 666–669.
2. Radisavljevic, B.; Radenovic, A.; Brivio, J.; Giacometti, V.; Kis, A. Single-Layer MoS_2 Transistors. *Nat. Nanotechnol.* **2011**, *6*, 147–150.
3. Dean, C. R.; Young, A. F.; Meric, I.; Lee, C.; Wang, L.; Sorgenfrei, S.; Watanabe, K.; Taniguchi, T.; Kim, P.; Shepard, K. L.; Hone, J. Boron Nitride Substrates for High-Quality Graphene Electronics. *Nat. Nanotechnol.* **2010**, *5*, 722–726.
4. Britnell, L.; Gorbachev, R. V.; Jalil, R.; Belle, B. D.; Schedin, F.; Mishchenko, A.; Georgiou, T.; Katsnelson, M. I.; Eaves, L.; Morozov, S. V.; Peres, N. M. R.; Leist, J.; Geim, A. K.; Novoselov, K. S.; Ponomarenko, L. A. Field-Effect Tunneling Transistor Based on Vertical Graphene Heterostructures. *Science* **2012**, *335*, 947–950.
5. Georgiou, T.; Jalil, R.; Belle, B. D.; Britnell, L.; Gorbachev, R. V.; Morozov, S. V.; Kim, Y.; Gholinia, A.; Haigh, S. J.; Makarovsky, O.; Eaves, L.; Ponomarenko, L. A.; Geim, A. K.; Novoselov, K. S.; Mishchenko, A. Vertical Field-Effect Transistor Based on Graphene-WS_2 Heterostructures for Flexible and Transparent Electronics. *Nat. Nanotechnol.* **2013**, *8*, 100–103.
6. Yu, W. J.; Liu, Y.; Zhou, H.; Yin, A.; Li, Z.; Huang, Y.; Duan, X. Highly Efficient Gate-Tunable Photocurrent Generation in Vertical Heterostructures of Layered Materials. *Nat. Nanotechnol.* **2013**, *8*, 952–958.
7. Britnell, L.; Ribeiro, R. M.; Eckmann, A.; Jalil, R.; Belle, B. D.; Mishchenko, A.; Kim, Y.; Gorbachev, R. V.; Georgiou, T.; Morozov, S. V.; Grigorenko, A. N.; Geim, A. K.; Casiraghi, C.; Neto, A. H. C.; Novoselov, K. S. Strong Light-Matter Interactions in Heterostructures of Atomically Thin Films. *Science* **2013**, *340*, 1311–1314.
8. Yu, W. J.; Li, Z.; Zhou, H.; Chen, Y.; Wang, Y.; Huang, Y.; Duan, X. Vertically Stacked Multi-Heterostructures of Layered Materials for Logic Transistors and Complementary Inverters. *Nat. Mater.* **2013**, *12*, 246–252.
9. Roy, K.; Padmanabhan, M.; Goswami, S.; Sai, T. P.; Ramalingam, G.; Raghavan, S.; Ghosh, A. Graphene-MoS_2 Hybrid Structures for Multifunctional Photoresponsive Memory Devices. *Nat. Nanotechnol.* **2013**, *8*, 826–830.
10. Choi, M. S.; Lee, G.; Yu, Y.; Lee, D.; Lee, S. H.; Kim, P.; Hone, J.; Yoo, W. J. Controlled Charge Trapping by Molybdenum Disulphide and Graphene in Ultrathin Heterostructured Memory Devices. *Nat. Commun.* **2013**, *4*, 1624.
11. Lee, G.; Yu, Y.; Cui, X.; Petrone, N.; Lee, C.; Choi, M. S.; Lee, D.; Lee, C.; Yoo, W. J.; Watanabe, K.; Taniguchi, T.; Nuckolls, C.; Kim, P.; Hone, J. Flexible and Transparent MoS_2 Field-Effect Transistors on Hexagonal Boron Nitride-Graphene Heterostructures. *ACS Nano* **2013**, *7*, 7931–7936.
12. Li, Y.; Xu, C.; Hu, P.; Zhen, L. Carrier Control of MoS_2 Nanoflakes by Functional Self-Assembled Monolayers. *ACS Nano* **2013**, *7*, 7795–7804.
13. Fang, H.; Tosun, M.; Seol, G.; Chang, T. C.; Takei, K.; Guo, J.; Javey, A. Degenerate n-Doping of Few-Layer Transition Metal Dichalcogenides by Potassium. *Nano Lett.* **2013**, *13*, 1991–1995.
14. Lin, J.; Zhong, J.; Zhong, S.; Li, H.; Zhang, H.; Chen, W. Modulating Electronic Transport Properties of MoS_2 Field Effect Transistor by Surface Overlayers. *Appl. Phys. Lett.* **2013**, *103*, 063109.

15. Du, Y.; Liu, H.; Neal, A. T.; Si, M.; Ye, P. D. Molecular Doping of Multilayer Field-Effect Transistors: Reduction in Sheet and Contact Resistances. *IEEE Electron Device Lett.* **2013**, *34*, 1328–1330.
16. Yun, J.; Noh, Y.; Yeo, J.; Go, Y.; Na, S.; Jeong, H.; Kim, J.; Lee, S.; Kim, S.; Koo, H. Y.; Kim, T.; Kim, D. Efficient Work-Function Engineering of Solution-Processed MoS_2 Thin-Films for Novel Hole and Electron Transport Layers Leading to High-Performance Polymer Solar Cells. *J. Mater. Chem. C* **2013**, *1*, 3777–3783.
17. Shi, Y.; Huang, J.; Jin, L.; Hsu, Y.; Yu, S. F.; Li, L.; Yang, H. Y. Selective Decoration of Au Nanoparticles on Monolayer MoS_2 Single Crystals. *Sci. Rep.* **2013**, *3*, 1839.
18. Mak, K. F.; Lee, C.; Hone, J.; Shan, J.; Heinz, T. F. Atomically Thin MoS_2: A New Direct-Gap Semiconductor. *Phys. Rev. Lett.* **2010**, *105*, 136805.
19. Yin, Z.; Li, H.; Li, H.; Jiang, L.; Shi, Y.; Sun, Y.; Lu, G.; Zhang, Q.; Chen, X.; Zhang, H. Single-Layer MoS_2 Phototransistors. *ACS Nano* **2012**, *6*, 74–80.
20. Lopez-Sanchez, O.; Lembke, D.; Kayci, M.; Radenovic, A.; Kis, A. Ultrasensitive Photodetectors Based on Monolayer MoS_2. *Nat. Nanotechnol.* **2013**, *8*, 497–501.
21. Choi, W.; Cho, M. Y.; Konar, A.; Lee, J. H.; Cha, G.; Hong, S. C.; Kim, S.; Kim, J.; Jena, D.; Joo, J.; Kim, S. High-Detectivity Multilayer MoS_2 Phototransistors with Spectral Response from Ultraviolet to Infrared. *Adv. Mater.* **2012**, *24*, 5832–5836.
22. Jariwala, D.; Sangwan, V. K.; Wu, C.; Prabhumirashi, P. L.; Geier, M. L.; Marks, T. J.; Lauhon, L. J.; Hersam, M. C. Gate-Tunable Carbon Nanotube-MoS_2 Heterojunction p-n Diode. *Proc. Natl. Acad. Sci.* **2013**, *110*, 18076–18080.
23. Fontana, M.; Deppe, T.; Boyd, A. K.; Rinzan, M.; Liu, A. Y.; Paranjape, M.; Barbara, P. Electron-Hole Transport and Photovoltaic Effect in Gated MoS_2 Schottky Junctions. *Sci. Rep.* **2013**, *3*, 1634.
24. Esmaeili-Rad, M.; Salahuddin, S. High Performance Molybdenum Disulfide Amorphous Silicon Heterojunction Photodetector. *Sci. Rep.* **2013**, *3*, 2345.
25. Lemme, M. C.; Koppens, F. H. L.; Falk, A. L.; Rudner, M. S.; Park, H.; Levitov, L. S.; Marcus, C. M. Gate-Activated Photoresponse in a Graphene p-n Junction. *Nano Lett.* **2011**, *11*, 4134–4137.
26. Mueller, T.; Xia, F.; Avouris, P. Graphene Photodetectors for High-Speed Optical Communications. *Nat. Photonics* **2010**, *4*, 297–301.
27. Liu, Y.; Cheng, R.; Liao, L.; Zhou, H.; Bai, J.; Liu, G.; Liu, L.; Huang, Y.; Duan, X. Plasmon Resonance Enhanced Multicolour Photodetection by Graphene. *Nat. Commun.* **2011**, *2*, 579.
28. Xia, F.; Mueller, T.; Lin, Y.; Valdes-Garcia, A.; Avouris, P. Ultrafast Graphene Photodetector. *Nat. Nanotechnol.* **2009**, *4*, 839–843.
29. Dean, C.; Young, A. F.; Wang, L.; Meric, I.; Lee, G.-; Watanabe, K.; Taniguchi, T.; Shepard, K.; Kim, P.; Hone, J. Graphene Based Heterostructures. *Solid State Commun.* **2012**, *152*, 1275–1282.
30. Shin, H.; Choi, W. M.; Choi, D.; Han, G. H.; Yoon, S.; Park, H.; Kim, S.; Jin, Y. W.; Lee, S. Y.; Kim, J. M.; Choi, J.; Lee, Y. H. Control of Electronic Structure of Graphene by Various Dopants and Their Effects on a Nanogenerator. *J. Am. Chem. Soc.* **2010**, *132*, 15603–15609.
31. Shi, Y.; Kim, K. K.; Reina, A.; Hofmann, M.; Li, L.; Kong, J. Work Function Engineering of Graphene Electrode *via* Chemical Doping. *ACS Nano* **2010**, *4*, 2689–2694.
32. Berry, V. Impermeability of Graphene and Its Applications. *Carbon* **2013**, *62*, 1–10.
33. Das, S.; Appenzeller, J. Where Does the Current Flow in Two-Dimensional Layered Systems? *Nano Lett.* **2013**, *13*, 3396–3402.
34. Li, S.; Wakabayashi, K.; Xu, Y.; Nakaharai, S.; Komatsu, K.; Li, W.; Lin, Y.; Aparecido-Ferreira, A.; Tsukagoshi, K. Thickness-Dependent Interfacial Coulomb Scattering in Atomically Thin Field-Effect Transistors. *Nano Lett.* **2013**, *13*, 3546–3552.
35. Atwater, H. A.; Polman, A. Plasmonics for Improved Photovoltaic Devices. *Nat. Mater.* **2010**, *9*, 205–213.
36. Chen, L.; Pan, C. Photoresponsivity Enhancement of ZnO/Si Photodiodes Through Use of an Ultrathin Oxide Interlayer. *Eur. Phys. J. Appl. Phys.* **2008**, *44*, 43–46.
37. Hazra, P.; Singh, S. K.; Jit, S. Ultraviolet Photodetection Properties of ZnO/Si Heterojunction Diodes Fabricated by ALD Technique without Using a Buffer Layer. *J. Semicond. Technol. Sci.* **2014**, *14*, 117–123.
38. Choi, Y. S.; Lee, J. Y.; Im, S.; Lee, S. J. Photoresponse Characteristics of n-ZnO/p-Si Heterojunction Photodiodes. *J. Vac. Sci. Technol. B* **2002**, *20*, 2384–2387.
39. Lee, S. H.; Lee, D.; Hwang, W. S.; Hwang, E.; Jena, D.; Yoo, W. J. High-Performance Photocurrent Generation from Two-Dimensional WS_2 Field-Effect Transistors. *Appl. Phys. Lett.* **2014**, *104*, 193113.